

Original Article

Preclinical development and characterisation of ^{99m}Tc-NM-01 for SPECT/CT imaging of human PD-L1

Nicholas CL Wong^{1*}, Yina Cai^{1*}, Levente K Meszaros¹, Hans-Jürgen Biersack², Gary JR Cook^{3,4}, Hong Hoi Ting¹, Felix M Mottaghy^{5,6}

¹NanoMab Technology Limited, Shanghai, People's Republic of China; ²Department of Nuclear Medicine, University Hospital Bonn, Bonn, Germany; ³King's College London and Guy's and St Thomas' PET Centre, St Thomas' Hospital, London, SE1 7EH, UK; ⁴Cancer Imaging, School of Biomedical Engineering and Imaging Sciences, Kings College London, London SE1 7EH, UK; ⁵Department of Nuclear Medicine, University Hospital RWTH Aachen, Germany; ⁶Department of Radiology and Nuclear Medicine, Maastricht University Medical Centre, Maastricht, The Netherlands. *Equal contributors.

Received March 22, 2021; Accepted May 22, 2021; Epub June 15, 2021; Published June 30, 2021

Abstract: The level of expression of programmed cell death-1 (PD-1)/programmed death ligand-1 (PD-L1) is a predictive biomarker for cancer immunotherapy, however, its detection remains challenging due to tumour heterogeneity and the influence from the binding of therapeutic agents. We recently developed [^{99m}Tc]-NM-01 as a companion diagnostic imaging agent for non-invasive molecular imaging of PD-L1 by single-photon emission computed tomography (SPECT). The aim of the study was to evaluate the [^{99m}Tc] radiolabelling of GMP graded NM-01 and its pharmacology, pharmacokinetics and toxicology. NM-01 bound specifically to human PD-L1 ($K_d=0.8$ nM) and did not interfere with the binding of the anti-PD-L1 antibody atezolizumab. NM-01 can bind various PD-L1-positive cancer cell lines and only interact with PD-L1 expressed on the cell surface. In SPECT/CT imaging, high [^{99m}Tc]-NM-01 accumulation was observed in the HCC827 mouse xenografted tumour model (30-min: 1.50 ± 0.27 %ID/g; 90-min: 1.23 ± 0.18 %ID/g), demonstrated a predominantly renal elimination (high uptake in bladder and kidney), while activity in the blood pool and other major organs remained low. The tumour-to-muscle and tumour-to-blood ratios were comparable with/without atezolizumab ($P<0.04$) but were significantly lowered when co-injected with excess NM-01 ($P=0.04$ and $P=0.01$, respectively.) The blood clearance of [^{99m}Tc]-NM-01 is bi-phasic; consisting of an initial fast washout phase with half-life of 2.1 min and a slower clearance phase with half-life of 25.4 min. In an intravenous extended single-dose toxicity study, no treatment-related changes were observed and the maximum tolerated dose of [^{99m}Tc]-NM-01 was 2.58 mg/kg. [^{99m}Tc]-NM-01 has suitable properties as a potential candidate for SPECT/CT imaging of PD-L1 assessment in cancer patients.

Keywords: PD-L1, radiolabelling, single domain antibody, SPECT/CT imaging, tracer

Introduction

Immunotherapy has advanced greatly in the past decade for the treatment of cancers. Several cancer entities have the potential to escape from recognition by the immune system by hijacking the immune checkpoints that prevent autoimmunity with excessive inhibitory signals during T-cell regulation [1-3]. PD-L1 is one of the ligands of PD-1 expressed by various types of cancer cells [4]. The binding of PD-L1 to PD-1 primarily occurs within inflamed tissues and in the tumour microenvironment where it

leads to down regulation on T-cells and reduced immunity. Blocking PD-1 or PD-L1 leads to preferential activation of cytotoxic T-cells with specificity for cancer cells [3, 5]. PD-1 and PD-L1 have been reported to be overexpressed in various solid tumours including non-small-cell lung cancer (NSCLC) and melanoma [6-8].

Several immune checkpoint inhibitors have been granted regulatory approval over the past few years for the treatment of different PD-L1-positive malignancies, when PD-L1 expression is confirmed by immunohistochemical evalua-

tion (IHC) of a tumour biopsy specimen [9-13]. Multiple clinical trials of other immune checkpoint inhibitors targeting the PD-1/PD-L1 pathway have reported a positive correlation between PD-L1 expression and response to treatment or overall survival [14-18]. Some studies, however, reported no correlation between PD-L1 expression and response to anti-PD-(L)1 immunotherapies [19-24]. Recent studies revealed that intra-/inter-tumoural heterogeneity possibly caused by differential T-cell infiltration and the differences in the definition of PD-L1 positivity and IHC methodology used across studies may be the reason behind this inconsistency [25-27].

Molecular imaging of PD-L1 offers an alternative, non-invasive and whole-body approach that resolves the practical issues encountered with IHC and has the potential in visualising intra-/inter-tumoural heterogeneity. Several clinical studies using [⁸⁹Zr]-atezolizumab, a radiolabelled anti-PD-L1 mAb; [¹⁸F]-BMS-986192 and [^{99m}Tc]-NM-01 have demonstrated a proof-of-concept for the potential of PD-L1 imaging by SPECT or positron emission tomography (PET). Tracer uptake in the clinical studies were all correlated with PD-L1 expression determined by IHC [6, 8, 28]. Obviously, the clinical responses in patients with atezolizumab treatment were even better correlated with [⁸⁹Zr]-atezolizumab uptake than with IHC or RNA sequencing based predictive markers [6, 8]. However, challenges remain for using therapeutic mAb based imaging tracers due to their slow clearance from the blood stream and normal tissue as well as its interaction with the treatment regimen [29-31].

Single-domain antibodies (sdAbs) are the smallest antigen-binding fragments derived from heavy-chain immunoglobulin (Ig)G from camel and show great promise for molecular imaging in numbers of preclinical and clinical studies because of their better tissue permeation and faster blood clearance [32-36]. We have screened and selected an anti-human PD-L1 sdAb, NM-01, that does not interfere with the PD-1/PD-L1 interaction as it binds to a different PD-L1 epitope from the binding site of common anti-PD-L1 mAbs. This would enable imaging to monitor PD-L1 expression before, during and after anti-PD-1/PD-L1 treatment.

In this study, we sought to develop a site-specific PD-L1 imaging agent radiolabelled with [^{99m}Tc] for SPECT/CT which can give good imaging results within one to two hours after injection, and will not interfere with the PD-1/PD-L1 interaction or share a binding site with existing therapeutic anti-PD-L1 mAbs agents. This would provide an alternative robust and affordable method to IHC for guiding immunotherapy.

Materials and methods

The preparation of anti-human PD-L1 sdAb NM-01

The anti-human PD-L1 sdAb, NM-01, was screened and selected from phage display library generated from peripheral blood lymphocytes of *Camelus bactrianus* immunised against human PD-L1 extracellular domain protein as previously described procedures [37, 38]. The NM-01 cloned in pMECs with a C-terminal HA-hexahistidine tag were transformed into non-suppressor strain WK6 cells and purified from periplasmic extract using affinity chromatography on a Ni-sepharose resin column (GE Healthcare, Pittsburgh, PA, USA).

ELISA

Microtiter plates were coated with human PD-L1 ECD-Fc or mouse PD-L1 ECD-Fc (R&D systems, Minneapolis, MN). To prevent non-specific binding, the plates were blocked with 1% bovine serum albumin (BSA) at room temperature for 2 h. sdAbs (descending concentrations from 200 nM) were added to the plates and incubated at room temperature for 1 h, followed by incubation with anti-HA antibody (Biolegend, San Diego, CA, USA) for 1 h and anti-mouse IgG-alkaline phosphatase (Proteintech, Rosemont, IL, USA) for another hour for detection. After the addition of TMB solution (eBioscience, San Diego, CA, USA) and H₂SO₄, absorbance at 450 nm was recorded on a Bio-Tek Synergy microplate reader.

Surface plasmon resonance (SPR)

The binding kinetics of sdAbs to immobilised human PD-L1 ECD-Fc were analysed by SPR on CM5 sensor chips using Biacore® 3000 system (GE Healthcare, Pittsburgh, PA, USA). The anti-

gen was coupled on a CM5 chip to 1000 resonance units (RU) with an amine coupling kit using the standard amine coupling procedure. The sdAbs were injected at 30 μ l/min in HBS-EP buffer at 25°C with binding for 180 s and dissociation for 720 s. The chip was regenerated in 25 mM NaOH for 60 s. The curves were locally fitted with BIA evaluation version 4.1 using a 1:1 Langmuir binding mode. The association and dissociation rates were monitored, and the equilibrium dissociation constant (K_d) was calculated. For competition experiments, the sdAbs and atezolizumab analogue (Crownbio Science, China) were sequentially injected either alone or in combination at 30 μ l/min in HBS-EP buffer in two 180 s binding phases. The curves were analysed using BIA evaluation version 4.1 and visually interpreted.

Cell lines and culture conditions

Human lung cancer (HCC827 and A549), liver (Hep 3B and SNU-423), gastric cancer (Hs764T and SNU-5.5), ovarian cancer (ES-2 and OVCAR-3), pancreatic cancer (BxPC-3 and ASPC-1), oesophageal cancer (KYSE-150 and KYSE-270) and breast cancer (MDA-MB-231 and BT474) cell lines were purchased from ATCC and cultured as recommended by the supplier.

Flow cytometry

Cells were harvested with a non-enzymatic cell dissociation buffer (Cell Stripper[®]; Corning, NY, USA). Cell suspensions containing 2×10^6 cells/ml in PBS were incubated at 4°C in the dark with FcR blocking reagent for 15 min (Miltenyi Biotec, Germany) to reduce non-specific binding; followed by sdAbs (30 min) and Alexa Fluor 488 anti-HA antibody (Biolegend, San Diego, CA, USA) for 20 min. The cells were washed twice with PBS between each step. Flow cytometry analyses were performed on a FACSCalibur flow cytometer (BD Biosciences, UK).

Effect of NM-01 on the PD-1/PD-L1 interaction

The effect of NM-01 on the PD-1/PD-L1 interaction was studied using PD-1 [Biotinylated]: PD-L1 Inhibitor Screening ELISA Assay Pair kit (ACRO Biosystems, China) according to the instructions provided by the manufacturer. Briefly, biotinylated PD-1 was incubated with immobilised human PD-L1 in the presence of increasing amounts (1–32 nM) of sdAbs or anti-

PD-1 mAb and using streptavidin-horseradish peroxidase and optical density detection at 450 nm.

The off-target binding screening of NM-01

The specificity of NM-01 to PD-L1 was evaluated using microarray technology (Retrogenix Ltd., UK) in a three-step screening process as previously described [39]. Assay optimisation was performed in a set of pre-screens. This was followed by primary screening: 2 μ g/ml of NM-01 was screened for binding against HEK293 cells individually expressing 5484 full-length plasma membrane and secreted proteins fixed on microarray slides (16 slide sets, $n=3$ slides per slide set). Each transfected cell line co-expressed ZsGreen1 for identification. The primary hits were identified by analysing fluorescent signal intensities (AF647 and ZsGreen1) in ImageQuant (GE Healthcare, Pittsburgh, PA, USA). NM-01 binding to individual antigens was assessed using anti-HA detection (AlexaFluor 647 labelled anti-HA detection antibody; Thermo Fisher, UK) or anti-His detection (Penta His AlexaFluor 647 conjugate; Qiagen, UK). Vectors encoding all hits were sequenced to confirm their correct identities. Confirmation/Specificity screen: Expression vectors encoding all primary hits and control sequences including CD86, EGFR and undefined PD-L1 isoform (del1-9) were prepared in duplicate on new slides similarly to the primary screening. Identical fixed slide sets were treated with 2 μ g/ml of NM-01, 1 μ g/ml of CTLA4-Fc/His (R&D systems, Minneapolis, MN, USA) or PBS ($n=2$ slides per treatment) followed by anti-HA or anti-His detection.

The GMP production and purification of NM-01

The nucleotide sequence of NM-01 was recloned into the expression vector pE7 with kanamycin resistance. The recombinant plasmid was transfected into the *E. coli* strain BLR (DE3) and a clone with high sdAb expression was used to establish the cell bank. NM-01 was purified from the periplasmic extract using cation-exchange chromatography (CIEX) on SP Sepharose Fast Flow (GE Healthcare, Pittsburgh, PA, USA), buffer-exchanged to phosphate buffer saline (PBS) by size exclusion chromatography (SEC) using Sephadex G-75 (GE Healthcare, Pittsburgh, PA, USA), concentrated

to 2.0 mg/ml, aliquoted in glass vials and stored at -20°C. Production was carried out in compliance with Annex 13.3 of Directive 2001/20/EC of the European Parliament and of the Council. The GMP graded NM-01 was used for radiolabelling and determination of shelf-life, *in vivo* imaging, blood clearance and determination of toxicity.

*The radiolabelling of NM-01 with [^{99m}Tc] with the [^{99m}Tc(OH)₂(CO)₃]⁺ core: radiochemical characterisation and quality control, *in vitro* stability and shelf-life*

Radiolabelling and quality control of NM-01 was performed following a previously published protocol [28], with some modifications, i.e. upon reconstitution in 1.0 ml of sodium pertechnetate in physiological saline, the kit for preparation of the [^{99m}Tc]-triacquatricarbonyl-technetium(I) intermediate was incubated in a dry heating block for 20 minutes. Shelf-life of [^{99m}Tc]-NM-01 was determined in three development batches, after 4-fold dilution in saline and filtration through two interconnected 0.22 µm low protein binding syringe filters (Merck Millipore, Germany) into a 10 ml pyrogen-free evacuated vial. The preparation was incubated at room temperature and aliquots were analysed by high-performance liquid chromatography (HPLC) and instant thin layer chromatography (iTLC) after 2, 4 and 6 h.

Mouse models

A toxicity study was performed in normal male and female Swiss Crl:CD-1 mice. Female Balb/C nu/nu mice were used to assess blood clearance and SPECT/CT imaging. Inoculation of HCC827 xenografts was performed under sevoflurane anaesthesia: mice were subcutaneously injected with 100 µl HCC827 cell suspension, corresponding to 5×10⁶ live cells in 1:1 matrigel:PBS in the flank at shoulder level. Tumour growth and animal body weight were monitored twice a week; tumour size was calculated using the formula 0.52 * length * width². Approximately four weeks after inoculation, when the average xenograft size has reached 200 mm³, mice were randomly assigned to four groups for *in vivo* imaging and *ex vivo* pharmacokinetics studies. The toxicity study was approved by Wuxi AppTec institutional animal care and use committee. The rest of the animal studies were performed under a licence

approved by the National Animal Experiments Inspectorate under the Ministry of Environment and Food of Denmark.

SPECT/CT imaging and data analysis

Preclinical SPECT/CT imaging was performed in a nanoScan SPECT/CT system (Mediso, Hungary) in three groups of mice. Mice in Group 1 (n=6) were intravenously administered 19.2-41.2 MBq of [^{99m}Tc]-NM-01, corresponding to 10 µg of NM-01 in 150 µl of saline. Mice in Group 2 (n=6) were intravenously administered 18.9-44.6 MBq of [^{99m}Tc]-NM-01, corresponding to 200 µg of NM-01 in 150 µl of saline. Mice in Group 3 (n=6) were intravenously administered 2 mg of atezolizumab (Tecentriq; Roche, Switzerland) in 125 µl saline four days before SPECT/CT imaging to block PD-L1 in the xenografts. For SPECT/CT imaging, mice in Group 3 were administered 15.2-33.8 MBq of [^{99m}Tc]-NM-01, corresponding to 10 µg of NM-01 in 150 µl of saline. Whole-body SPECT/CT images were acquired 30-min and 90-min post-injection under sevoflurane anaesthesia.

In vivo blood clearance

In vivo blood clearance of [^{99m}Tc]-NM-01 was studied in a group of 5 mice bearing HCC827 xenografts. Mice were administered 10 MBq [^{99m}Tc]-NM-01, corresponding to 10 µg of NM-01 in 150 µl of saline in a lateral tail vein under terminal sevoflurane anaesthesia. Venous blood samples were collected from a contralateral tail vein at 1-, 5-, 10-, 20-, 40-, 60-, 90- and 120-min post-injection into 10 µl (± 0.5%) capillary tubes. Blood samples were measured in a calibrated gamma counter (Wizard2; Perkin Elmer, MA, USA) and the amount of radioactivity recovered from the blood pool was calculated at every time point based on the assumption that blood accounts for 8% of total body weight and the density of blood is 1 g/cm³.

Toxicity study with [^{99m}Tc]-NM-01

The toxicity of [^{99m}Tc]-NM-01 was assessed in an intravenous extended single-dose toxicity study in mice, conducted in compliance with good laboratory practice (GLP) guidelines set by the National Medical Products Administration (China) and Organisation for Economic Co-operation and Development (OECD). The full

materials and methods of the toxicity study are described in supplemental data. [^{99m}Tc]-NM-01 (corresponding to 80 µg NM-01 per mouse), prepared as described above and stored at 2-8°C for 11 days for radioactive decay, or 0.9% w/v NaCl solution for injection was administered i.v. in 20 male and 20 female CD-1 mice. Parameters including body weight and body weight change, food consumption, haematology, serum chemistry, organ weight, gross and microscopic pathology were monitored. One and fourteen days after injection, 10 mice per group (5 male and 5 female) were euthanised and underwent necropsy: up to 39 organs and tissues per mouse were collected for gross and histopathological evaluation. Samples and test results were reviewed by a veterinary pathologist certified by the American College of Veterinary Pathologists.

Statistical analysis

The ELISA results were fitted a nonlinear regression model with GraphPad Prism 6.0 (GraphPad, San Diego, CA, USA) to determine the K_d. The flow cytometry data were analysed with FlowJo (Tristar Inc., El Segundo, CA, USA). Radiochemical purities and identities in different time points were compared by two-sample unequal variance t-tests. Biodistribution of [^{99m}Tc]-NM-01 was calculated based on SPECT/CT images. Biodistribution in different time points and groups was compared by two-sample unequal variance t-tests. To calculate the biological blood half-life of [^{99m}Tc]-NM-01, a two-phase exponential fit with no constraints was performed in Prism (GraphPad Software). P value of less than 0.05 was considered as statistically significant.

Results

The characterisation of NM-01 against human PD-L1

The binding affinity and specificity of NM-01 were determined using recombinant PD-L1 protein in ELISA assays. NM-01 bound specifically to human PD-L1 with K_d at 1.8 nM, but not to mouse PD-L1 (**Figure 1A**). The binding kinetics were also confirmed using surface plasmon resonance (SPR). In SPR studies, NM-01 exhibited a strong affinity to human PD-L1 with sub-nanomolar affinity (K_d=0.8 nM) and the binding of NM-01 did not interfere with the binding of

atezolizumab to human PD-L1 (**Figure 1B**). In a competitive ELISA assay, it was found that NM-01 had no impact on the binding of PD-1 to PD-L1 while the positive control (anti-PD-1 mAb) inhibited the PD-1/PD-L1 interaction with an EC₅₀ of 5.6 nM (**Figure 1C**). The ability of NM-01 to bind human PD-L1 on cancer cell lines derived from solid tumours, including lung cancer, liver cancer, gastric cancer, ovarian cancer, pancreatic cancer, oesophageal cancer and breast cancer cell lines were further evaluated by flow cytometry. NM-01 was able to differentiate the PD-L1 expression on cancer cell lines from multiple cancers (**Figure 1D**).

The specificity of NM-01 to human PD-L1 was also assessed using a microarray-based binding assay to 5484 full-length plasma membrane and secreted proteins followed by anti-HA and anti-His detection (**Figure 2**). Primary screening identified nine primary (binding) hits and all of them were reproducibly observed in the confirmatory screen. Seven out of nine primary hits were excluded in the confirmatory screen as they were also observed in the control slides with phosphate buffered saline (PBS) or cytotoxic T-lymphocyte-associated protein (CTLA4)-Fc/His. Two hits, corresponding to human PD-L1 isoform 1 (full-length extracellular domain (ECD)) and isoform 2 (lacking IgV like domain), were confirmed as specific by both anti-HA and anti-His detection. No difference between the two detection methods was observed. These data confirmed the monospecificity and high affinity of NM-01 to human PD-L1.

The radiolabelling and characterisation of NM-01 with [^{99m}Tc] with the [^{99m}Tc(OH)₂(CO)₃]⁺ core

The results of the stability study of GMP-graded NM-01 indicated that no change in concentration or biological activity and no protein degradation takes place for at least 6 months at 25°C and at least 18 months at -20°C (**Tables S1** and **S2**).

[^{99m}Tc]-NM-01 was successfully produced on all occasions with radiochemical purity (RCP)>90%. Three batches of [^{99m}Tc]-NM-01 were prepared to confirm the shelf-life of the radiotracer and the reproducibility of the radiolabelling results. Specific radioactivity of the three batches was 7507 ± 290 MBq/mg (106 ± 4 MBq/nmol) at the end of synthesis and the

^{99m}Tc -NM-01 for PD-L1 SPECT/CT imaging

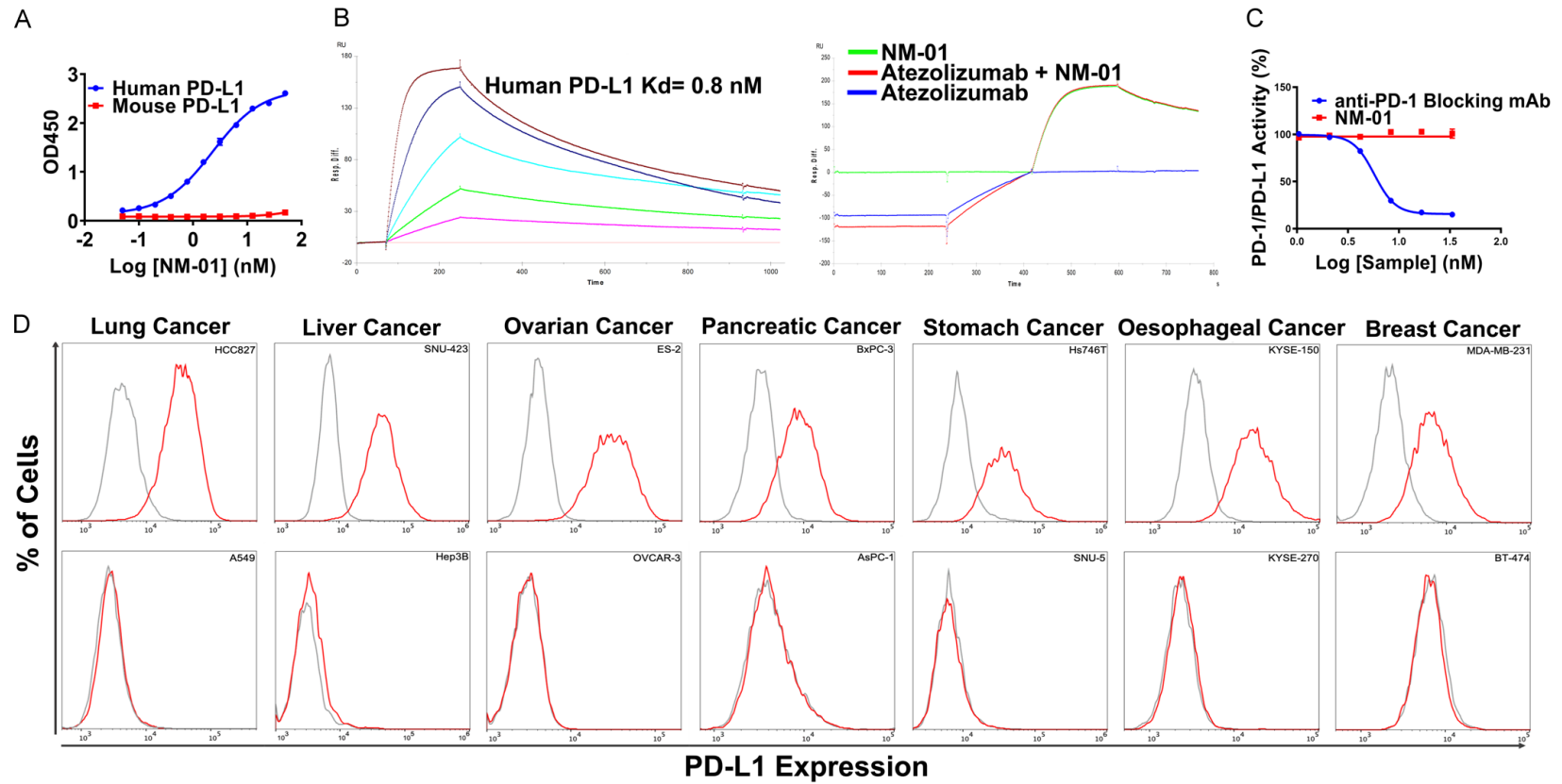


Figure 1. The characterisation of NM-01. A. The binding affinity of NM-01 to human and mouse and PD-L1 as determined by ELISA assays. B. The binding kinetics of NM-01 at different doses and with or without the presence of atezolizumab as determined by SPR. C. The impact of NM-01 on the inhibitory effect of atezolizumab as determined by a competitive ELISA assay. D. The binding ability of NM-01 to PD-L1 on different cancer cell lines as determined by flow cytometry.

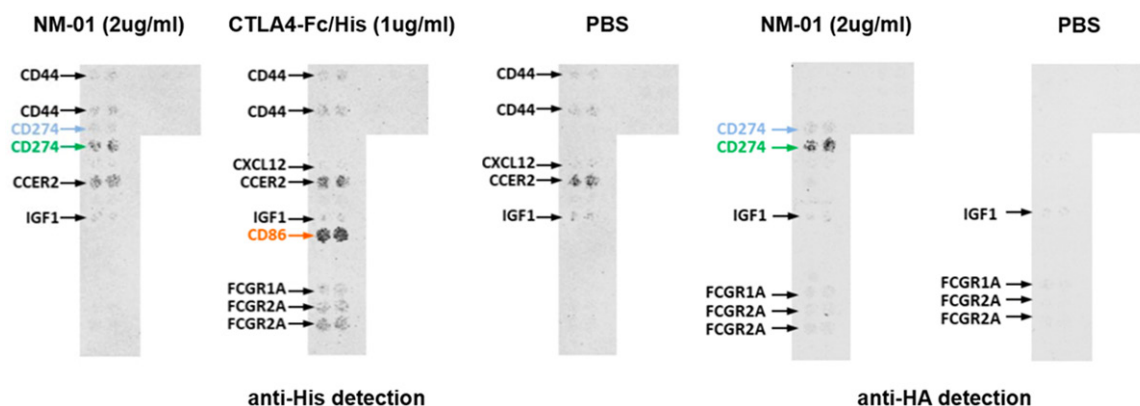


Figure 2. The specificity of NM-01 as determined by microarray-based binding assays followed by anti-HA and anti-His detection, with CTLA4-Fc/His and PBS served as control slides.

average RCP of these batches, as determined by iTLC and HPLC, were $96.4 \pm 1.6\%$ and $95.6 \pm 1.6\%$ respectively. No significant changes in RCP or protein degradation were observed with iTLC (RCP at 6 hr = $96.7 \pm 2.0\%$, $P < 0.92$) or HPLC (RCP at 6 hr = $97.6 \pm 0.8\%$, $P < 0.22$) upon incubation at room temperature for at least 6 h (Table S3).

SPECT/CT imaging

SPECT/CT imaging was performed in mice bearing subcutaneous, PD-L1-positive HCC827 xenografts. High [^{99m}Tc]-NM-01 accumulation was observed in the urinary bladder and kidneys while uptake in the blood pool (represented by the heart) and other major organs such as the lungs, liver and skeletal muscle remained low (Figure 3A). [^{99m}Tc]-NM-01 uptake was observed in the PD-L1-positive HCC827 xenografts (Group 1, 1.50 ± 0.27 %ID/g at 30-min and 1.23 ± 0.18 %ID/g at 90-min). Co-injection with excess NM-01 (Group 2) partially offset [^{99m}Tc]-NM-01 accumulation in the tumour to 0.84 ± 0.28 %ID/g at 30-min and 0.60 ± 0.14 %ID/g at 90-min post-injection. In both time points, [^{99m}Tc]-NM-01 uptake in Group 2 was significantly lower than in the respective time point in Group 1 ($P < 0.001$). Pre-dosing mice with 2 mg atezolizumab (Group 3) did not interfere with [^{99m}Tc]-NM-01 uptake in the tumour; uptake in the xenograft was 1.57 ± 0.10 %ID/g at 30-min and 1.33 ± 0.09 %ID/g at 90-min post-injection (Figure 3B). No statistically significant difference could be established in [^{99m}Tc]-NM-01 uptake between Group 1 and Group 3 in either time point ($P > 0.25$) (Figure 4).

Blood clearance of [^{99m}Tc]-NM-01

The %ID recovered from the blood pool of five mice between 1- to 120-min post-injection was presented in Figure S1. By 1-min post-injection, approximately 75% of injected radioactivity cleared from the blood pool. By 120-min post-injection, less than 2 %ID could be recovered from the blood pool. To determine the biological blood half-life of [^{99m}Tc]-NM-01, a two-phase exponential fit was performed. In the fast phase, 69% of the drug product was cleared from the blood pool with a half-life of 2.1 min and the remaining 31% was cleared with a half-life of 25.4 min in the slow phase.

Toxicity study of [^{99m}Tc]-NM-01

In an intravenous extended single-dose toxicity study in mice, no treatment-related changes were observed in any of the monitored parameters, including body weight, food consumption, haematology, serum chemistry, organ weight, macroscopic and microscopic observations at both day 2 (n=20) and day 14 (n=20). The maximum tolerated dose (MTD) of [^{99m}Tc]-NM-01 in this study was 80 µg/animal, corresponding to an average dose of approximately 2.58 mg/kg.

Discussion

In the present study, we developed an anti-PD-L1 sdAb imaging agent that 1) is monospecific to human PD-L1 with excellent pharmacokinetics; 2) does not interfere with existing anti-PD-L1 mAbs therapeutic agents and 3) radiolabels site specifically with [^{99m}Tc] for *in vivo* PD-L1

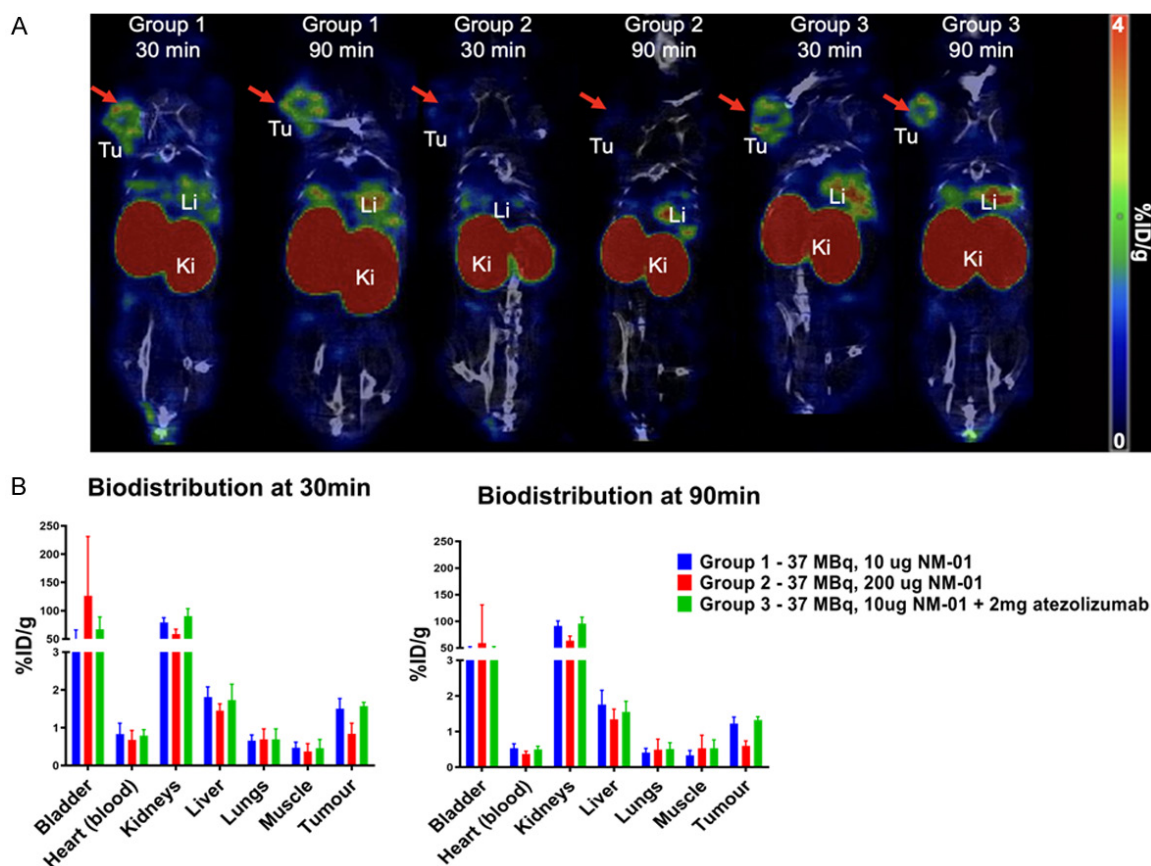


Figure 3. The biodistribution of [^{99m}Tc]-NM-01 in mice. A. The representative image of [^{99m}Tc]-NM-01 in mice bearing subcutaneous, PD-L1-positive HCC827 xenografts injected with [^{99m}Tc]-NM-01 (Group 1); co-injection of excess NM-01 (Group 2); and pre-dosing with 2 mg atezolizumab (Group 3) as assessed by SPECT/CT imaging at 30-min and 90-min post-injection. B. Comparison of the image-derived uptake of [^{99m}Tc]-NM-01 in major organs at 30-min and 90-min post-injection.

imaging with SPECT/CT. This allows the longitudinal measurement of PD-L1 expression before, during and after anti-PD-1/PD-L1 treatment.

Different IHC methodology have been implemented in clinical practice to assess tumour PD-L1 expression for the selection of patients for immune checkpoint inhibitors. However, it is becoming clear that tumour PD-L1 expression is heterogeneous within and between tumours and changes in response to treatment over time [40, 41]. It is extremely challenging to take biopsy from multiple sites simultaneously and repeatedly for the accurate assessment of PD-L1 expression. A clinical study using [⁸⁹Zr]-atezolizumab demonstrated that pre-treatment PET scan appeared to be a better predictor of response to atezolizumab than IHC but it required imaging to be performed 7 days after tracer injection for optimal imaging results

(Tumour-to-blood ratios increased from around 1 to 5 between day 2 to day 7) [6]. To improve biodistribution and clearance, several investigators have explored protein engineering approaches, including the use of sdAbs and other protein scaffolds [42-46].

We screened and selected NM-01 from phage display library generated from camelus bactrianus immunised against human PD-L1. NM-01 is highly specific to human PD-L1 with good binding affinity in ELISA and SPR comparable with other reported PD-L1 sdAbs [42, 44]. Competitive SPR assays with atezolizumab analogues confirmed that the binding epitope of NM-01 on PD-L1 is different from that of the mAb. A competitive ELISA assay with biotinylated PD-1 demonstrated that NM-01 did not interfere with the PD-1/PD-L1 interaction like the sdAb K2 presented by Broos et al. [42]. Off-

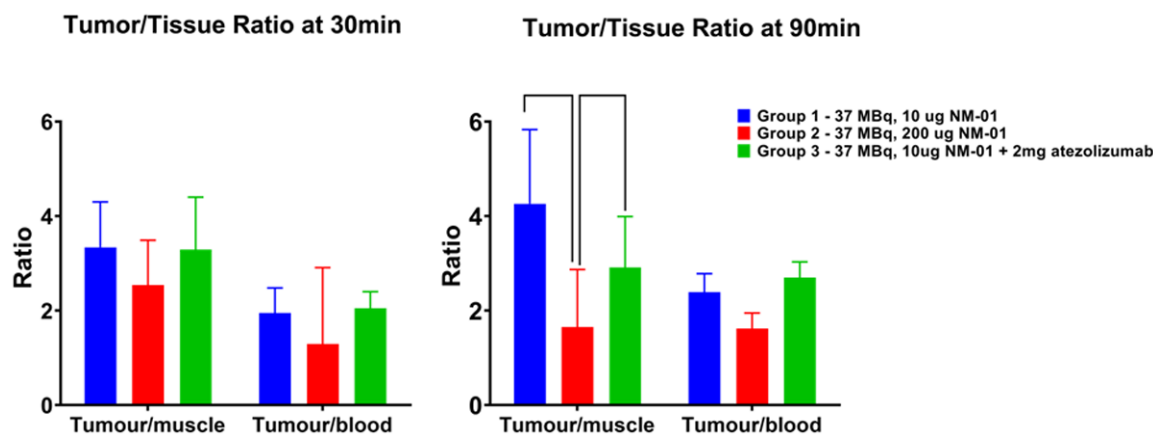


Figure 4. Comparison of tumour-to-muscle or tumour-to-blood ratios at 30-min and 90-min post-injection. Significant difference in tumour-to-muscle ratios was found between Group 1 vs Group 2 and Group 2 vs Group 3 at 90-min post-injection ($P=0.04$ and $P=0.01$, respectively). Tumour-to-blood ratios at both time points were significantly higher in Groups A and C compared to Group 2 ($P<0.04$). No statistically significant difference could be established in tumour-to-muscle or tumour-to-blood ratios between Group 1 and Group 3 at either time point ($P>0.05$).

target screening of NM-01 using microarray expressing 5484 full-length plasma membrane and secreted proteins validated the monospecificity as well as safety of NM-01, which supports NM-01 a suitable candidate for rapid clinical translation.

We manufactured GMP-grade NM-01 with comparable stability to a previously reported sdAb [47]. The GMP produced NM-01 was radiolabelled with ^{99m}Tc site specifically in a two-step method under GMP condition. The radiolabelling efficiency was always above 90% and purification after radiolabelling was not necessary. Several factors affect and determine the kinetics of triaquatricarbonyltechnetium(I) binding to the His-tag, for example, protein (i.e. His-tag) concentration in the labelling mixture, ionic strength of the labelling mixture and the amino acid sequence in the vicinity of the His-tag [48-50]. Considering these findings and the fact that protein sequences are not always reported, the comparability of radiolabelling efficiencies may sometimes be challenging. ^{99m}Tc -NM-01 has a shelf-life at ambient temperature of at least 6 h. This allows time for the distribution ^{99m}Tc -NM-01 from centralised radiopharmacies as well as on-site labelling at any standard hospital radiopharmacy, and enables the widespread use of NM-01 in monitoring treatment response in patients undergoing immunotherapy in clinical setting.

SPECT/CT imaging in mice bearing PD-L1-positive xenografts confirmed that ^{99m}Tc -

NM-01 uptake was PD-L1 mediated since the excess amount of NM-01 (Group 2) significantly offset ^{99m}Tc -NM-01 uptake. With no statistically significant difference established between Group 1 and Group 3, the latter group pre-dosed with the anti-PD-L1 mAb atezolizumab, we confirmed in vivo that the binding epitope of NM-01 and atezolizumab on PD-L1 are different, providing further evidence that using ^{99m}Tc -NM-01 for the imaging of PD-L1-positive malignancies in cancer patients will not affect the therapeutic effect of anti-PD-1/PD-L1 antibodies and the use of such antibodies will not interfere with imaging using ^{99m}Tc NM-01.

^{99m}Tc -NM-01 demonstrated very rapid blood clearance due to rapid renal extraction and urinary excretion. This is expected for a small hydrophilic protein of this size, similar to other radiolabelled sdAbs [42, 44]. Although biodistribution of ^{99m}Tc -NM-01 was very similar to that of other radiolabelled sdAbs, uptake in the xenograft, and consequently tumour-to-background ratios were markedly lower than values reported for another PD-L1 targeting sdAbs, ^{99m}Tc -sdAb K2 and ^{68}Ga -NOTA-Nb109; albeit still significantly higher than in control groups [42, 44]. This difference in tumour uptake is most probably due to the fact that Broos et al. and Lv et al. used PD-L1 transfected xenograft models for in vivo evaluation and transfected cell lines are likely to express higher levels of PD-L1 than HCC827 cells used in this study (Figure S2). Other than ^{99m}Tc -NM-01, ^{18}F -BMS-986192 is the only comparable

small protein that has been evaluated in cancer patients. In preclinical studies, the tumour to blood ratios reported with [¹⁸F]-BMS-986192 in NSCLC xenograft model L2987 were comparable to [^{99m}Tc]-NM-01 at 90 min post injection. The kidney and lung uptake of with [¹⁸F]-BMS-986192 were relatively high although the authors did not report biodistribution results in non-target organs in %ID/g or SUV units making direct comparison impossible [43]. The clinical translation of [¹⁸F]-BMS-986192 demonstrated positive correlation between PD-L1 expression determined by PET/CT IHC in most NSCLC patients [8]. The heterogeneity of PD-L1 expression between and within patients was observed. Similar observations were found in the early phase I study of [^{99m}Tc]-NM-01 in NSCLC patients [28].

In a single-dose toxicology study, the MTD of [^{99m}Tc]-NM-01 in CD-1 mice was 80 µg/animal, corresponding to a dose of 2.58 mg/kg. With a species-specific uncertainty factor of 12 taken into account, this corresponds to a human-equivalent MTD of 215 µg/kg, which is approximately 150 times higher than the preferable human dose of a new radiopharmaceutical (below 100 µg or 1.4 µg/kg for an average body weight of 70 kg), confirming the safety use of [^{99m}Tc]-NM-01 for PD-L1 imaging in human [51]. No tracer-related adverse events have been reported in the 32 patients received the injection of [^{99m}Tc]-NM-01 up to date (unpublished data).

To conclude, [^{99m}Tc]-NM-01 is a promising candidate for SPECT/CT imaging of PD-L1 expression in cancer patients, with appropriate binding specificity, kinetic and toxicity profiles. It has been evaluated in an early phase I study for NSCLC cancer imaging and shown to be safe with acceptable dosimetry (NCT02978196) [28]. [^{99m}Tc]-NM-01 may be particularly useful for monitoring anti-PD-L1 therapy since it does not share a binding site with common anti-PD-L1 antibodies. It is currently undergoing another clinical trial for the evaluation of PD-L1 expression in NSCLC and melanoma patients before and after immunotherapy (NCT044-36406). It has also been approved for a phase 2 clinical trial to evaluate the correlation between PD-L1 imaging and PD-L1 IHC as well as blood tumour mutation burden (EudraCT-2020-002809-26). The on-going clinical trials

will help to establish the baseline of PD-L1 expression within and between patients and tumour types, a cut-off point for patient selection and treatment monitoring.

Acknowledgements

We thank Minerva Imaging (Olstykke, Denmark) for the technical assistance on the imaging of [^{99m}Tc]-NM-01. We also thank Retrogenix Ltd (Chinley, UK) for the technical assistance on the off-target binding screening with microarray.

Disclosure of conflict of interest

N.C.L.W., Y.C., L.K.M. and H.H.T. are employees of NanoMab Technology Ltd. H.J.B. is an advisor for NanoMab Technology Ltd. G.J.R.C. is a consultant and receive research support for NanoMab Technology Ltd, Theragnostics Ltd and Serac Healthcare Ltd. F. M. M is on the advisory board of Advanced Accelerator Applications GmbH and has received institutional grants from GE Healthcare, Siemens, and NanoMab Technology Ltd.

Address correspondence to: Felix M Mottaghy, Department of Nuclear Medicine, University Hospital RWTH Aachen, Anstalt des öffentlichen Rechts (AöR), Pauwelsstrasse 30, 52074 Aachen, Germany. E-mail: fmottaghy@ukaachen.de

References

- [1] Marhelava K, Pilch Z, Bajor M, Graczyk-Jarzynka A and Zagodzón R. Targeting negative and positive immune checkpoints with monoclonal antibodies in therapy of cancer. *Cancers (Basel)* 2019; 11: 1756.
- [2] Okazaki T and Honjo T. PD-1 and PD-1 ligands: from discovery to clinical application. *Int Immunol* 2007; 19: 813-824.
- [3] Pardoll DM. The blockade of immune checkpoints in cancer immunotherapy. *Nat Rev Cancer* 2012; 12: 252-264.
- [4] Freeman GJ, Long AJ, Iwai Y, Bourque K, Chernova T, Nishimura H, Fitz LJ, Malenkovich N, Okazaki T, Byrne MC, Horton HF, Fouser L, Carter L, Ling V, Bowman MR, Carreno BM, Collins M, Wood CR and Honjo T. Engagement of the PD-1 immunoinhibitory receptor by a novel B7 family member leads to negative regulation of lymphocyte activation. *J Exp Med* 2000; 192: 1027-1034.
- [5] Ribas A. Tumor immunotherapy directed at PD-1. *N Engl J Med* 2012; 366: 2517-9.

- [6] Bensch F, van der Veen EL, Lub-de Hooge MN, Jorritsma-Smit A, Boellaard R, Kok IC, Oosting SF, Schröder CP, Hiltermann TJN, van der Wekken AJ, Groen HJM, Kwee TC, Elias SG, Gietema JA, Bohorquez SS, de Crespigny A, Williams SP, Mancao C, Brouwers AH, Fine BM and de Vries EGE. (89)Zr-atezolizumab imaging as a non-invasive approach to assess clinical response to PD-L1 blockade in cancer. *Nat Med* 2018; 24: 1852-1858.
- [7] Gatalica Z, Snyder C, Maney T, Ghazalpour A, Holterman DA, Xiao N, Overberg P, Rose I, Basu GD, Vranic S, Lynch HT, Von Hoff DD and Hamid O. Programmed cell death 1 (PD-1) and its ligand (PD-L1) in common cancers and their correlation with molecular cancer type. *Cancer Epidemiol Biomarkers Prev* 2014; 23: 2965-2970.
- [8] Niemeijer AN, Leung D, Huisman MC, Bahce I, Hoekstra OS, van Dongen G, Boellaard R, Du S, Hayes W, Smith R, Windhorst AD, Hendrikse NH, Poot A, Vugts DJ, Thunnissen E, Morin P, Lipovsek D, Donnelly DJ, Bonacorsi SJ, Velasquez LM, de Gruijl TD, Smit EF and de Langen AJ. Whole body PD-1 and PD-L1 positron emission tomography in patients with non-small-cell lung cancer. *Nat Commun* 2018; 9: 4664.
- [9] Gandhi L, Rodríguez-Abreu D, Gadgeel S, Esteban E, Felip E, De Angelis F, Domine M, Clingan P, Hochmair MJ, Powell SF, Cheng SY, Bischoff HG, Peled N, Grossi F, Jennens RR, Reck M, Hui R, Garon EB, Boyer M, Rubio-Viqueira B, Novello S, Kurata T, Gray JE, Vida J, Wei Z, Yang J, Raftopoulos H, Pietanza MC and Garassino MC; KEYNOTE-189 Investigators. Pembrolizumab plus chemotherapy in metastatic non-small-cell lung cancer. *N Engl J Med* 2018; 378: 2078-2092.
- [10] Herbst RS, Baas P, Kim DW, Felip E, Perez-Gracia JL, Han JY, Molina J, Kim JH, Arvis CD, Ahn MJ, Majem M, Fidler MJ, de Castro G Jr, Garrido M, Lubiniecki GM, Shentu Y, Im E, Dolled-Filhart M and Garon EB. Pembrolizumab versus docetaxel for previously treated, PD-L1-positive, advanced non-small-cell lung cancer (KEYNOTE-010): a randomised controlled trial. *Lancet* 2016; 387: 1540-1550.
- [11] Mok TSK, Wu YL, Kudaba I, Kowalski DM, Cho BC, Turna HZ, Castro G Jr, Srimuninnimit V, Laktionov KK, Bondarenko I, Kubota K, Lubiniecki GM, Zhang J, Kush D and Lopes G; KEYNOTE-042 Investigators. Pembrolizumab versus chemotherapy for previously untreated, PD-L1-expressing, locally advanced or metastatic non-small-cell lung cancer (KEYNOTE-042): a randomised, open-label, controlled, phase 3 trial. *Lancet* 2019; 393: 1819-1830.
- [12] Nosaki K, Saka H, Hosomi Y, Baas P, de Castro G Jr, Reck M, Wu YL, Brahmer JR, Felip E, Sawada T, Noguchi K, Han SR, Piperdi B, Kush DA and Lopes G. Safety and efficacy of pembrolizumab monotherapy in elderly patients with PD-L1-positive advanced non-small-cell lung cancer: pooled analysis from the KEYNOTE-010, KEYNOTE-024, and KEYNOTE-042 studies. *Lung Cancer* 2019; 135: 188-195.
- [13] Paz-Ares L, Luft A, Vicente D, Tafreshi A, Gümüş M, Mazières J, Hermes B, Çay Şenler F, Csósz T, Fülöp A, Rodríguez-Cid J, Wilson J, Sugawara S, Kato T, Lee KH, Cheng Y, Novello S, Halmos B, Li X, Lubiniecki GM, Piperdi B and Kowalski DM; KEYNOTE-407 Investigators. Pembrolizumab plus chemotherapy for squamous non-small-cell lung cancer. *N Engl J Med* 2018; 379: 2040-2051.
- [14] Borghaei H, Paz-Ares L, Horn L, Spigel DR, Steins M, Ready NE, Chow LQ, Vokes EE, Felip E, Holgado E, Barlesi F, Kohlhaufl M, Arrieta O, Burgio MA, Fayette J, Lena H, Poddubskaya E, Gerber DE, Gettinger SN, Rudin CM, Rizvi N, Crino L, Blumenschein GR Jr, Antonia SJ, Dorange C, Harbison CT, Graf Finckenstein F and Brahmer JR. Nivolumab versus docetaxel in advanced nonsquamous non-small-cell lung cancer. *N Engl J Med* 2015; 373: 1627-1639.
- [15] Brahmer JR, Drake CG, Wollner I, Powderly JD, Picus J, Sharfman WH, Stankevich E, Pons A, Salay TM, McMiller TL, Gilson MM, Wang C, Selby M, Taube JM, Anders R, Chen L, Korman AJ, Pardoll DM, Lowy I and Topalian SL. Phase I study of single-agent anti-programmed death-1 (MDX-1106) in refractory solid tumors: safety, clinical activity, pharmacodynamics, and immunologic correlates. *J Clin Oncol* 2010; 28: 3167-3175.
- [16] Ferris RL and Licitra L. Nivolumab in patients with recurrent or metastatic squamous cell carcinoma of the head and neck: efficacy and safety in checkmate 141 by prior cetuximab use. *Clin Cancer Res* 2019; 25: 5221-5230.
- [17] Motzer RJ, Rini BI, McDermott DF, Redman BG, Kuzel TM, Harrison MR, Vaishampayan UN, Drabkin HA, George S, Logan TF, Margolin KA, Plimack ER, Lambert AM, Waxman IM and Hammers HJ. Nivolumab for metastatic renal cell carcinoma: results of a randomized phase II trial. *J Clin Oncol* 2015; 33: 1430-1437.
- [18] Rosenberg JE, Hoffman-Censits J, Powles T, van der Heijden MS, Balar AV, Necchi A, Dawson N, O'Donnell PH, Balmanoukian A, Loriot Y, Srinivas S, Retz MM, Grivas P, Joseph RW, Galsky MD, Fleming MT, Petrylak DP, Perez-Gracia JL, Burris HA, Castellano D, Canil C, Bellmunt J, Bajorin D, Nickles D, Bourgon R, Frampton GM, Cui N, Mariathasan S, Abidoye O, Fine GD and Dreicer R. Atezolizumab in patients with locally

- advanced and metastatic urothelial carcinoma who have progressed following treatment with platinum-based chemotherapy: a single-arm, multicentre, phase 2 trial. *Lancet* 2016; 387: 1909-1920.
- [19] Brahmer J, Reckamp KL, Baas P, Crino L, Eberhardt WE, Poddubskaya E, Antonia S, Pluzanski A, Vokes EE, Holgado E, Waterhouse D, Ready N, Gainor J, Aren Frontera O, Havel L, Steins M, Garassino MC, Aerts JG, Domine M, Paz-Ares L, Reck M, Baudalet C, Harbison CT, Lestini B and Spigel DR. Nivolumab versus docetaxel in advanced squamous-cell non-small-cell lung cancer. *N Engl J Med* 2015; 373: 123-135.
- [20] Carbognin L, Pilotto S, Milella M, Vaccaro V, Brunelli M, Calio A, Cuppone F, Sperduti I, Giannarelli D, Chilosì M, Bronte V, Scarpa A, Bria E and Tortora G. Differential activity of nivolumab, pembrolizumab and MPDL3280A according to the tumor expression of programmed death-ligand-1 (PD-L1): sensitivity analysis of trials in melanoma, lung and genitourinary cancers. *PLoS One* 2015; 10: e0130142.
- [21] Carbone DP, Reck M, Paz-Ares L, Creelan B, Horn L, Steins M, Felip E, van den Heuvel MM, Ciuleanu TE, Badin F, Ready N, Hiltermann TJN, Nair S, Juergens R, Peters S, Minenza E, Wrangle JM, Rodriguez-Abreu D, Borghaei H, Blumenschein GR Jr, Villaruz LC, Havel L, Krejci J, Corral Jaime J, Chang H, Geese WJ, Bhagavatheeswaran P, Chen AC, Socinski MA and CheckMate I. First-line nivolumab in stage IV or recurrent non-small-cell lung cancer. *N Engl J Med* 2017; 376: 2415-2426.
- [22] Motzer RJ, Escudier B, McDermott DF, George S, Hammers HJ, Srinivas S, Tykodi SS, Sosman JA, Procopio G, Plimack ER, Castellano D, Choueiri TK, Gurney H, Donskov F, Bono P, Wagstaff J, Gaurer TC, Ueda T, Tomita Y, Schutz FA, Kollmannsberger C, Larkin J, Ravaud A, Simon JS, Xu LA, Waxman IM, Sharma P and CheckMate I. Nivolumab versus everolimus in advanced renal-cell carcinoma. *N Engl J Med* 2015; 373: 1803-1813.
- [23] Reck M, Rodriguez-Abreu D, Robinson AG, Hui R, Czoszi T, Fulop A, Gottfried M, Peled N, Tafreshi A, Cuffe S, O'Brien M, Rao S, Hotta K, Leiby MA, Lubiniecki GM, Shentu Y, Rangwala R and Brahmer JR. Pembrolizumab versus chemotherapy for PD-L1-positive non-small-cell lung cancer. *N Engl J Med* 2016; 375: 1823-1833.
- [24] Rittmeyer A, Barlesi F, Waterkamp D, Park K, Ciardiello F, von Pawel J, Gadgeel SM, Hida T, Kowalski DM, Dols MC, Cortinovis DL, Leach J, Polikoff J, Barrios C, Kabbinar F, Frontera OA, De Marinis F, Turna H, Lee JS, Ballinger M, Kowanetz M, He P, Chen DS, Sandler A and Gandara DR; OAK Study Group. Atezolizumab versus docetaxel in patients with previously treated non-small-cell lung cancer (OAK): a phase 3, open-label, multicentre randomised controlled trial. *Lancet* 2017; 389: 255-265.
- [25] Anceviski Hunter K, Socinski MA and Villaruz LC. PD-L1 testing in guiding patient selection for PD-1/PD-L1 inhibitor therapy in lung cancer. *Mol Diagn Ther* 2018; 22: 1-10.
- [26] Haragan A, Field JK, Davies MPA, Escriu C, Gruver A and Gosney JR. Heterogeneity of PD-L1 expression in non-small cell lung cancer: implications for specimen sampling in predicting treatment response. *Lung Cancer* 2019; 134: 79-84.
- [27] Kim DH, Kim H, Choi YJ, Kim SY, Lee JE, Sung KJ, Sung YH, Pack CG, Jung MK, Han B, Kim K, Kim WS, Nam SJ, Choi CM, Yun M, Lee JC and Rho JK. Exosomal PD-L1 promotes tumor growth through immune escape in non-small cell lung cancer. *Exp Mol Med* 2019; 51: 1-13.
- [28] Xing Y, Chand G, Liu C, Cook GJR, O'Doherty J, Zhao L, Wong NCL, Meszaros LK, Ting HH and Zhao J. Early phase I study of a (^{99m}Tc)-labeled anti-programmed death ligand-1 (PD-L1) single-domain antibody in SPECT/CT assessment of PD-L1 expression in non-small cell lung cancer. *J Nucl Med* 2019; 60: 1213-1220.
- [29] Ehlerding EB, Lee HJ, Barnhart TE, Jiang D, Kang L, McNeel DG, Engle JW and Cai W. Noninvasive imaging and quantification of radiotherapy-induced PD-L1 upregulation with (⁸⁹Zr)-Df-Atezolizumab. *Bioconjug Chem* 2019; 30: 1434-1441.
- [30] Josefsson A, Nedrow JR, Park S, Banerjee SR, Rittenbach A, Jammes F, Tsui B and Sgouros G. Imaging, biodistribution, and dosimetry of radionuclide-labeled PD-L1 antibody in an immunocompetent mouse model of breast cancer. *Cancer Res* 2016; 76: 472-479.
- [31] Lesniak WG, Chatterjee S, Gabrielson M, Lisok A, Wharram B, Pomper MG and Nimmagadda S. PD-L1 detection in tumors using [(64)Cu] Atezolizumab with PET. *Bioconjug Chem* 2016; 27: 2103-10.
- [32] Keyaerts M, Xavier C, Heemskerk J, Devoogdt N, Everaert H, Ackaert C, Vanhoeij M, Duhoux FP, Gevaert T and Simon P. Phase I study of ⁶⁸Ga-HER2-nanobody for PET/CT assessment of HER2 expression in breast carcinoma. *J Nucl Med* 2016; 57: 27-33.
- [33] uVaneycken I, Devoogdt N, Van Gassen N, Vincke C, Xavier C, Wernery U, Muyldermans S, Lahoutte T and Cavelliers V. Preclinical screening of anti-HER2 nanobodies for molecular imaging of breast cancer. *FASEB J* 2011; 25: 2433-2446.

- [34] Xavier C, Vaneycken I, D’huyvetter M, Heemskerk J, Keyaerts M, Vincke C, Devoogdt N, Muyltermans S, Lahoutte T and Caveliers V. Synthesis, preclinical validation, dosimetry, and toxicity of ⁶⁸Ga-NOTA-anti-HER2 Nanobodies for iPET imaging of HER2 receptor expression in cancer. *J Nucl Med* 2013; 54: 776-784.
- [35] Zhou Z, Vaidyanathan G, McDougald D, Kang CM, Balyasnikova I, Devoogdt N, Ta AN, McNaughton BR and Zalutsky MR. Fluorine-18 labeling of the HER2-targeting single-domain antibody 2Rs15d using a residualizing label and preclinical evaluation. *Mol Imaging Biol* 2017; 19: 867-877.
- [36] Debie P, Lafont C, Defrise M, Hansen I, van Willigen DM, van Leeuwen FWB, Gijssbers R, D’Huyvetter M, Devoogdt N, Lahoutte T, Mollard P and Hernot S. Size and affinity kinetics of nanobodies influence targeting and penetration of solid tumours. *J Control Release* 2020; 317: 34-42.
- [37] Zhu M, Gong X, Hu Y, Ou W and Wan Y. Streptavidin-biotin-based directional double Nanobody sandwich ELISA for clinical rapid and sensitive detection of influenza H5N1. *J Transl Med* 2014; 12: 352.
- [38] Zhu M, Hu Y, Li G, Ou W, Mao P, Xin S and Wan Y. Combining magnetic nanoparticle with biotinylated nanobodies for rapid and sensitive detection of influenza H3N2. *Nanoscale Res Lett* 2014; 9: 528.
- [39] Freeth J and Soden J. New advances in cell microarray technology to expand applications in target deconvolution and off-target screening. *SLAS Discov* 2020; 25: 223-230.
- [40] Frederick DT, Piris A, Cogdill AP, Cooper ZA, Lezcano C, Ferrone CR, Mitra D, Boni A, Newton LP, Liu C, Peng W, Sullivan RJ, Lawrence DP, Hodi FS, Overwijk WW, Lizée G, Murphy GF, Hwu P, Flaherty KT, Fisher DE and Wargo JA. BRAF inhibition is associated with enhanced melanoma antigen expression and a more favorable tumor microenvironment in patients with metastatic melanoma. *Clin Cancer Res* 2013; 19: 1225-31.
- [41] Guo L, Song P, Xue X, Guo C, Han L, Fang Q, Ying J, Gao S and Li W. Variation of programmed death ligand 1 expression after platinum-based neoadjuvant chemotherapy in lung cancer. *J Immunother* 2019; 42: 215-220.
- [42] Broos K, Lecocq Q, Xavier C, Bridoux J, Nguyen TT, Corthals J, Schoonooghe S, Lion E, Raes G, Keyaerts M, Devoogdt N and Breckpot K. Evaluating a single domain antibody targeting human PD-L1 as a nuclear imaging and therapeutic agent. *Cancers (Basel)* 2019; 11: 872.
- [43] Donnelly DJ, Smith RA, Morin P, Lipovšek D, Gokemeijer J, Cohen D, Lafont V, Tran T, Cole EL, Wright M, Kim J, Pena A, Kukral D, Dischino DD, Chow P, Gan J, Adalakun O, Wang XT, Cao K, Leung D, Bonacorsi SJ Jr and Hayes W. Synthesis and biological evaluation of a novel ¹⁸F-labeled adnectin as a PET radioligand for imaging PD-L1 expression. *J Nucl Med* 2018; 59: 529-535.
- [44] Lv G, Qiu L, Sun Y, Li K, Liu Q, Zhao Q, Qin S and Lin J. PET imaging of tumor PD-L1 expression with a highly specific non-blocking nanobody. *J Nucl Med* 2020; 61: 117-122.
- [45] Maute RL, Gordon SR, Mayer AT, McCracken MN, Natarajan A, Ring NG, Kimura R, Tsai JM, Manglik A, Kruse AC, Gambhir SS, Weissman IL and Ring AM. Engineering high-affinity PD-1 variants for optimized immunotherapy and immuno-PET imaging. *Proc Natl Acad Sci U S A* 2015; 112: E6506-E6514.
- [46] González Trotter DE, Meng X, McQuade P, Rubins D, Klimas M, Zeng Z, Connolly BM, Miller PJ, O’Malley SS, Lin SA, Getty KL, Fayadat-Dilman L, Liang L, Wahlberg E, Widmark O, Ekblad C, Frejd FY, Hostetler ED and Evelhoch JL. In vivo imaging of the programmed death ligand 1 by ¹⁸F PET. *J Nucl Med* 2017; 58: 1852-1857.
- [47] Xavier C, Blykers A, Laoui D, Bolli E, Vaneycken I, Bridoux J, Baudhuin H, Raes G, Everaert H, Movahedi K, Van Ginderachter JA, Devoogdt N, Caveliers V, Lahoutte T and Keyaerts M. Clinical translation of [⁶⁸Ga]Ga-NOTA-anti-MMR-sdAb for PET/CT imaging of protumorigenic macrophages. *Mol Imaging Biol* 2019; 21: 898-906.
- [48] Badar A, Williams J, de Rosales RT, Tavaré R, Kampmeier F, Blower PJ and Mullen GE. Optimising the radiolabelling properties of technetium tricarbonyl and His-tagged proteins. *EJNMMI Res* 2014; 4: 14.
- [49] Waibel R, Alberto R, Willuda J, Finnern R, Schibli R, Stichelberger A, Egli A, Abram U, Mach JP and Plückthun A. Stable one-step technetium-99m labeling of His-tagged recombinant proteins with a novel Tc (I)-carbonyl complex. *Nat Biotechnol* 1999; 17: 897.
- [50] Williams JD, Kampmeier F, Badar A, Howland K, Cooper MS, Mullen GED and Blower PJ. Optimal his-tag design for efficient [(^{99m}Tc(CO)(3))(+) and [(¹⁸⁸Re(CO)(3))(+) labeling of proteins for molecular imaging and radionuclide therapy by analysis of peptide arrays. *Bioconjug Chem* 2020; [Epub ahead of print].
- [51] Nair AB and Jacob S. A simple practice guide for dose conversion between animals and human. *J Basic Clin Pharm* 2016; 7: 27-31.

^{99m}Tc-NM-01 for PD-L1 SPECT/CT imaging

Table S1. The results for the stability tests of GMP graded NM-01 at the recommended storage temperature (-20 ± 5 °C, results available up to 18 months)

Test items at 20 ± 5 °C	Acceptance criteria	Time (Months)							
		0	1	2	3	6	9	12	18
Protein content	2.0 mg/mL ± 10%	1.9	2.0	2.0	1.9	2.0	2.0	2.0	2.0
Purity-SE-HPLC	Main peak ≥95%	98.4	99.9	100.0	99.2	99.8	99.7	99.7	100.0
Biological activity	Kd<10 nM	5.3 nM	4.3 nM	4.1 nM	5.4 nM	2.5 nM	2.5 nM	1.5 nM	5.7 nM

Table S2. The results for the stability tests of GMP graded NM-01 under accelerated conditions (20 ± 5 °C, 60% relative humidity, results available for up to 6 months)

Test items at 20 ± 5 °C	Acceptance criteria	Time (Months)				
		0	1	2	3	6
Protein content	2.0 mg/mL ± 10%	1.9	2.0	2.1	1.9	2.0
Purity-SE-HPLC	Main peak ≥95%	98.4	98.4	99.0	97.9	100.0
Biological activity	Kd<10 nM	5.3 nM	4.6 nM	4.6 nM	7.4 nM	3.0 nM

Table S3. The results for the stability tests of [^{99m}Tc]-NM-01 at room temperature

Test items at RT	Acceptance criteria	Time (Hours)			
		0	2	4	6
RCP (iTLC)	Main peak >90%	96.4 ± 1.6	96.2 ± 3.4	96.0 ± 1.7	96.7 ± 2.0
RCP (HPLC)	Main peak >90%	95.6 ± 1.1	96.7 ± 1.1	97.2 ± 1.0	97.6 ± 0.8
pH	6-9	7.5	7.5	7.5	7.5
Endotoxin	≤175 EU/mL	<2.0	n.a	n.a	n.a
Sterility	Sterile	Conform	n.a	n.a	n.a

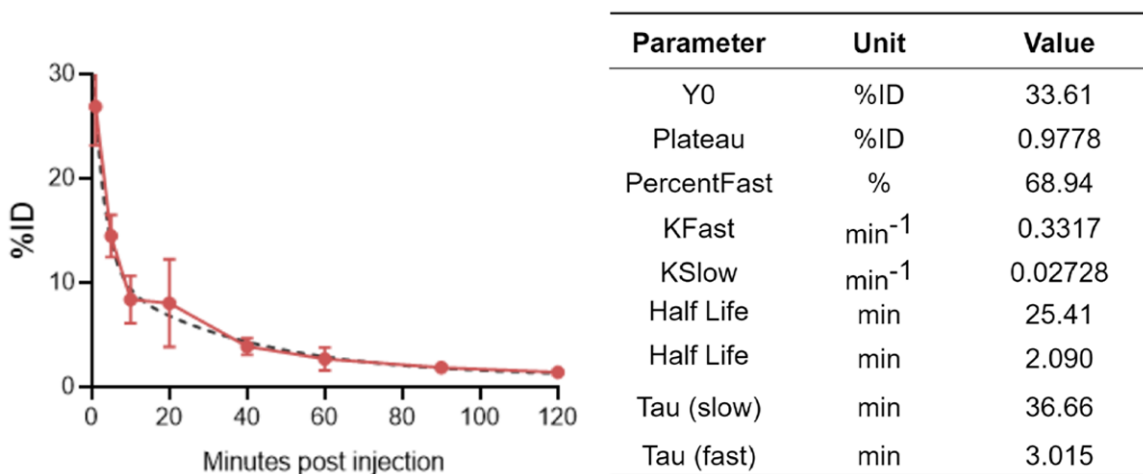


Figure S1. The blood clearance of [^{99m}Tc]-NM-01 in Balb/C nu/nu mice bearing HCC827 xenografts.

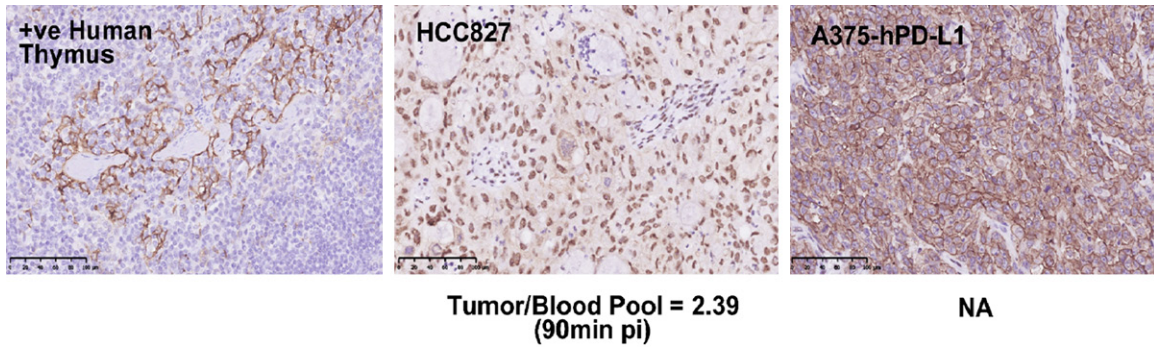


Figure S2. The PD-L1 IHC staining of a representative mouse xenograft tumour: a positive control tissue (human thymus); a HCC827 xenograft demonstrating PD-L1 staining and an A375-hPD-L1 transfected xenograft expressing high levels of human PD-L1 demonstrating strong staining.